CHEMISTRY OF MATERIALS

pubs.acs.org/cm

Article

Transition Metal Doping in CdS Quantum Dots: Diffusion, Magnetism, and Ultrafast Charge Carrier Dynamics

Saptarshi Chakraborty,[‖] Payel Mondal,[‖] Mahima Makkar, Luca Moretti, Giulio Cerullo, and Ranjani Viswanatha*

Cite This: *Chem. Mater.* 2023, 35, 2146–2154

Read Online

ACCESS | Metrics & More | Article Recommendations | Supporting Information

ABSTRACT: Transition metal (TM) doping in pristine II–VI semiconductor quantum dots (QDs) is known to add several otherwise unavailable properties by introducing midgap states in the host material. Albeit being extensively investigated, the periodicity of the observed properties with respect to the electronic structure has not been attempted so far. In this work, we investigate CdS QDs doped with several different TM ions (Mn, Fe, Co, Ni, and Cu) using extended X-ray absorption fine structure spectroscopy to study dopant-induced structural perturbations and femtosecond transient absorption (TA) spectroscopy to study the ultrafast charge carrier dynamics. This provides solid evidence for the origin of magnetization in doped QDs that has been lacking despite extensive studies. Further, we demonstrate that the ionic radius and the dopant oxidation state play crucial roles in determining the dopant–anion bond lengths. Based on the investigation of the relaxation pathways of excited charge carriers using ultrafast TA spectroscopy, we hypothesize that there exists photoinduced switching between multiple oxidation states in some dopants.

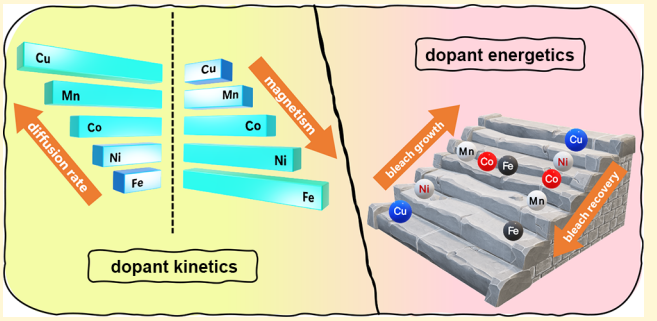

INTRODUCTION

TM doping in II–VI semiconductor QDs is one of the most widely explored problems in the field of semiconducting nanomaterials because of their unique optoelectronic, magnetic, magneto-optical properties and growth mechanisms.[1,2] Precise control over the host QDs' shape, size, and surface states in addition to the relative positioning of the dopant ions, achievable by colloidal synthesis, has enabled accurate dopant-induced tuning to harness properties beyond the reach of the pristine QDs. Nevertheless, these materials have opened up several gaps within our fundamental understanding in the areas of energetics, symmetry-forbidden transitions, and the origin of magnetism in these materials.

For example, the most widely explored TM dopants (Mn^{2+} and Cu^{2+}) are known to introduce midgap states in the II–VI QDs[3] that control the carrier dynamics of the pristine host, providing a new pathway for a dopant emission, thereby enabling a dual emissive QD.[4−10] Sensitization of Mn levels has been spectroscopically explained by the substitution of the divalent host cations in binary or ternary QDs by isoelectronic Mn^{2+} ions, leading to the ligand field transition in Mn^{2+}.[11−15] However, the underlying mechanism has been debated in the literature, and both energy and charge transfer from the host have been hypothesized.[16,17] Due to the intense photoluminescence (PL) and the relative insensitivity of Mn emission on the external perturbation, Mn excitation has been thought to occur through energy transfer.[18,19] However, the measurement of the rate of exciton–dopant energy transfer by transient absorption (TA) spectroscopy has revealed a substantially longer timescale than those typically associated with the energy transfer.[20,21] In addition, the timescale involved in the nonradiative hole trapping process (50–100 ps) has suggested a possible charge transfer. Though the charge transfer from the host to the Mn^{2+} dopant has been thought to be energetically unfavorable, recently, it has been shown that the transient Mn excited state (Mn^{3+}) is formed by a charge transfer from the host to the dopant.[15] However, direct experimental evidence of a transient Mn excited state is lacking.

Similarly, it has been hypothesized that the dilute magnetic semiconductor (DMS) contribution to the magnetism associated with the TM-doped systems plays a crucial role in dictating the magnetic properties. DMS materials are characterized by a small number of TM impurities, which are known to induce ferromagnetic ordering in otherwise non-

Received: December 22, 2022
Revised: February 10, 2023
Published: February 28, 2023

magnetic QDs[1,22] and are quite different compared to the bulk ferromagnetic materials. By incorporating open-shell TM dopants into II−VI semiconductors, DMS materials introduce localized unpaired spins that are magnetically coupled to delocalized charge carriers, where their coupling strengths depend on the dopant−carrier spatial overlap.[1] However, the nature of the magnetism depends on several factors including the number of dopants within a nanoparticle, the dopant location, and so on.[2] The origin of ferromagnetic ordering in DMS materials has so far been intensely debated. The main contenders include the dopant−carrier sp−d exchange, the formation of secondary magnetic phases, and the possibility of surface magnetism arising out of the dopant clustering.[23] The tools for studying the clustering of dopant atoms within these semiconductors are indirect and do not clearly distinguish between the magnetism arising from small clusters of dopants and the host. Fundamental thermodynamic questions like how the bond lengths should vary for different dopants within the same host or how the diffusivity of the dopants should change are yet to be understood. Similarly, although several reports have investigated the carrier dynamics in the individual TM-doped II−VI semiconductor QDs,[24−27] a comprehensive study that tries to harmonize the same of different TM dopants is still lacking.

To address these problems, several mechanistic studies have been performed, including the growth of the QDs, the diffusion of dopants within the solid matrix, and the photochemistry of the excited energy states. Additionally, ways to overcome synthesis challenges during the growth of QDs like self-purification[4,22] are still being studied. Lacking from these studies is the one tool from the toolkit of chemistry, namely, the periodicity of the properties. In this work, to answer these critical questions, we have studied the periodicity of properties within a simple system of CdS QDs doped with various TM dopants, namely, Mn, Fe, Co, Ni, and Cu. We have used extended X-ray absorption fine structure (EXAFS) spectroscopy to study their fundamental parameters like the bond lengths and coordination numbers (CNs) involved in the system. With these studies, we address two important loopholes, namely, the clustering and the transient oxidation state of the dopant ions. An estimate of the fraction of the dopants on the surface is used to quantify the number of dopant ions in the core of the QDs. This information is used to qualitatively predict magnetism and is verified with the data reported in previous studies. Based on the results, we conclude that the residual magnetism observed in these materials is indeed the result of host−dopant sp−d exchange and not surface magnetism arising out of the dopant clusters. We show that the ionic radii of the dopants are responsible for the dopant−sulfur interatomic distances, where the dopant oxidation state plays a crucial role. This result, obtained from the structural analysis, is correlated with the charge carrier relaxation pathways investigated via femtosecond TA spectroscopy, which shows conclusive evidence that some dopants (Mn and Co) can transiently switch between multiple oxidation states.

RESULTS AND DISCUSSION

All the samples were synthesized using the colloidal method via successive ion layer adsorption and reaction (SILAR) technique following the literature reports.[4,5] The brief description of the synthesis and structural characterization is provided in the Methods section. The formation of the QDs was characterized by X-ray diffraction patterns (XRD) and transmission electron microscopy (TEM). As shown in Figure S1a in the Supporting Information (SI), XRD patterns of doped QDs demonstrate the formation of the hexagonal CdS ($P6_3mc$) structure (Materials Project ID mp-672) similar to that of the bulk CdS without any impurity. Due to the small size of the QDs, the XRD peaks are broadened, consistent with the TEM images shown in Figures S1b−e. The study of energetics and magnetism requires careful attention to the synthesis procedure, where the dopants do not cluster and they should be present inside the QDs. The location of the dopants inside the host system obtained from the diffusion doping method discussed above has been extensively studied in earlier literature using various structural tools such as high-resolution TEM (HRTEM), scanning transmission electron microscopy, and EXAFS as well as indirectly through optical and magnetic properties.[4,5,28] It has been observed that in the range of dilute doping where the dopant concentration is low, dopants do not cause any major change in the host crystal structure, and hence, HRTEM does not show any discontinuity among the crystal planes. In this current work, similar to earlier literature, we observed that doped QDs do not show any crystal defects as shown by a typical HRTEM image of Mn-doped CdS QDs in Figure S2. The optical properties of QDs were characterized using UV−visible and steady-state PL spectroscopy. While UV−visible spectra show absorption onset at their respective bandgap energies, the steady-state PL spectra show the evolution of an intense broad dopant-related emission peak (except for Fe-doped CdS) along with the excitonic emission feature as shown in Figure S3, which also confirms the successful dilute substitutional doping of TM ions into the CdS host.

Although the observation of dopant-related emission peaks confirms doping, it does not give information on the local bonding environment. To evaluate the oxidation states of the dopants and their local coordination environments and hence their clustering, we studied the local structure of both Cd and the dopant atoms using X-ray absorption near edge structure (XANES) and EXAFS spectroscopy. All EXAFS data were processed in Athena and fitted in Artemis, part of the Demeter package.[29] Before going to the details of the EXAFS data, we present a brief theoretical overview of the bonds and bond lengths of interest in our system. The first coordination shell in pristine CdS consists of Cd atoms coordinated with 4 S atoms at an interatomic distance of 2.51 Å, and the second shell comprises 12 Cd atoms at 4.09 Å. The dopants M (M: Mn, Fe, Co, Ni, and Cu) are modeled to replace Cd substitutionally in the tetrahedral sites and do not occupy any interstitial position. The dopant_K edges were modeled replacing the Cd atoms with the dopant atoms changing the lattice parameters of pristine CdS obtained from the respective M−S bond lengths through an iterative fitting procedure briefly described in the Methods section.

XANES spectra are expected to provide information regarding the oxidation state of the metal ions along with the primary details of the bond purity. Figure S4a shows the XANES spectra of the Cd_K edge in doped and undoped QDs. The almost identical nature of the XANES spectra suggests that the oxidation state of Cd does not change with doping. The identical oscillations of the wavevector (k) shown in Figure S4b for the Cd_K edge for the doped and undoped QDs further confirm that the local bonding environments of all the samples are indistinguishable. To demonstrate this in an

https://doi.org/10.1021/acs.chemmater.2c03776
Chem. Mater. 2023, 35, 2146−2154

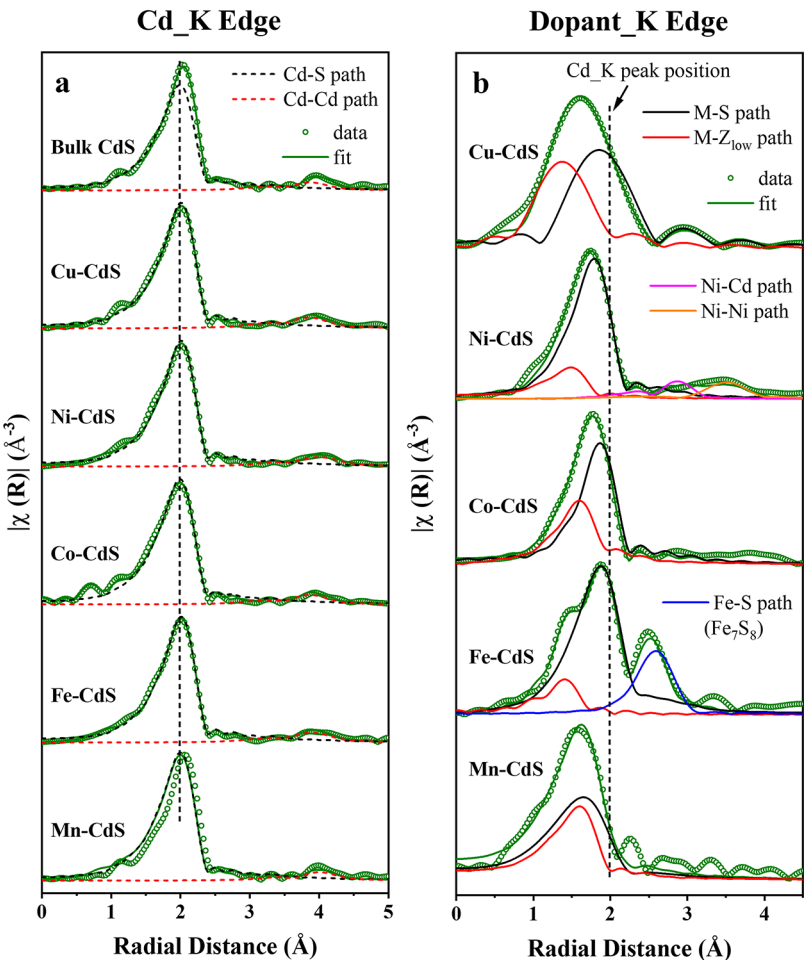

Figure 1. Magnitude of Fourier transformed (a) Cd_K edge and (b) dopant_K edge EXAFS spectra of TM-doped CdS with the bulk phase (hollow green circles) and best fits (green lines) along with the theoretical paths used for fitting. The dotted vertical line in both the panels marks the Cd−S bond length plotted to compare with the other M−S bond lengths.

intuitive obvious manner, we plot the magnitude of the k^3-weighted Fourier transformed EXAFS data for the Cd_K edge in real space in Figure 1a. As expected from the fitting of these scattering curves, all the samples have Cd−S interactions in their first coordination shells, represented by the peak around 2 Å, and a weaker Cd−Cd interaction around 4 Å. Notably, no Cd−dopant interactions were observed in any of the samples. As shown in the fitting summary in Table S1 in the SI, the first nearest neighbor of Cd (S) is coordinated to nearly 4 in all cases. Good quality global fits could be obtained for all the samples using these two paths and did not require any additional paths accounting for the surface states. This indicates that the Cd atoms reside in the core region of the QDs, and the samples do not have effective trap states. Thus, it suggests that the samples are mostly defect-free, and dopant-induced structural perturbation on the Cd sites is minimal to nonexistent, as expected in the dilute doping regime.

The dopant-induced perturbation, in question, should be expected in the doped samples since Cd^{2+} ($4d^{10}$) ions get replaced by the first-row transition metal ions having 3d configurations in substitutional doping. Under the same ligand environment, when ions of a 4d element (Cd^{2+}) get replaced by ions of 3d elements (Cu^{2+}/Ni^{2+}/Fe^{2+}, etc.), it leads to an increase in the charge density over the metal ions. Thus, in the case of doped QDs, the crystal field splitting is expected to be more as compared to the pristine CdS QDs. However, the dopant concentrations in all the cases are lower than 1% of the cation composition, and this effect is unlikely to be observed in our experiment. Nevertheless, since EXAFS spectroscopy is atom-specific and each dopant has separate core electron energy, the same is expected to give information on structural perturbation. Similar to Cd_K edge fittings, we fitted the dopant K (M_K) edges to quantify the local chemical environment around the dopants. The k^3-weighted Fourier transformed EXAFS data in the R-space of all dopant K (M_K) edges are presented in Figure 1b. The dopant K edge spectra are dominated by a single peak around 1.6−1.8 Å except for Fe-CdS suggesting a major contribution from one single bonding environment around the dopant ions. The presence of two peaks in Fe-CdS can be explained by the study of the synthesis procedure. All the samples were doped by diffusion-controlled growth of the M−S core, the dopants diffusing outward as the reaction progresses into the dilute limit.[28] However, the strong bond dissociation energy of Fe_7S_8 and the weak diffusion constant of Fe lead to the presence of a substantial amount of the Fe_7S_8 core even after a long reaction time. The presence of this core gives rise to the two-peak structure in EXAFS data, which was observed to vanish at later stages of growth in a previous study.[30] Except this, no other dopant−dopant interactions are present in the samples, suggesting that the doping is dilute, and clustering of the dopants is absent. However, the diffusivity of the dopants was

https://doi.org/10.1021/acs.chemmater.2c03776
Chem. Mater. 2023, 35, 2146−2154

found to vary for different host matrices. For example, Bürger and coworkers showed that depending on the substrate, the diffusion coefficient of Fe is greater (in the case of Si) or lower (for GaAs) than that of Mn.[31] Thus, the diffusivity of the dopants in CdS cannot be extrapolated from other materials. As the diffusion process is expected to play a key role in determining which dopants move out from the core toward the surface, an independent measure of the dopants on the surface could give us an idea of their diffusivity within the host matrix.

To obtain a qualitative measurement of the dopant diffusion through the QDs, further in-depth analysis of the dopant K edges (Figure 1b) was performed. The relevant parameters obtained by fitting the EXAFS data are listed in Table 1 below.

Table 1. EXAFS Model-Obtained CN, Bond Lengths (R), Literature-Reported Values (R_{lit}), and Normalized Area under the Peaks

sample	shell	CN	R (Å)	R_{lit} (Å)	normalized M−Z_{low} area
Mn-CdS	Mn−S	4.00	2.347	2.35[32]	0.427
Fe-CdS	Fe−S	3.43	2.392	2.39[30]	0.167
Co-CdS	Co−S	2.75	2.283	2.24[33]	0.355
Ni-CdS	Ni−S	3.84	2.277		0.201
Cu-CdS	Cu−S	0.92	2.309	2.32[34]	0.430

The data suggest that similar to the Cd_K edges, the first coordination sphere contains mainly M−S interactions; however, to obtain reasonable fits, each data set required the introduction of an M−Z_{low} path via quick shell fit in Artemis, wherein the Z_{low} is an element with a lower atomic number like oxygen or nitrogen, accounting for the fact that some of the dopant atoms are near the surface and hence coordinated with the ligands. The area under the curve of the M−Z_{low} peak normalized with respect to the total area of M−S and M−Z_{low} peaks (Table 1) quantifies the number of atoms engaged in the absorption (or scattering) process. This comparison yields the highest M−Z_{low} area for Cu, suggesting the fastest diffusivity. Since Cu, unlike the other dopants, was introduced at the growth stage and not during the core nucleation to avoid the precipitation of Cu precursors at high temperatures, the number of Cu atoms in the core of the QDs is expected to be small. This is closely followed by Mn and then Co, Ni, and Fe, respectively. Thus, it can be stated that Fe, with a slow diffusivity, resides mostly in the core region, whereas a non-negligible portion of Cu and Mn lies on the surface.

The number of dopants coordinated to the surface ligands would have a direct impact on the magnetism arising from the sp−d exchange interactions. Magnetism in nanomaterials is known to arise from different origins: from ferromagnetic metals, magnetic clusters embedded within the nonmagnetic clusters, surface defects,[35] and sp−d exchange in DMS QDs due to the orbital overlap of the host and the dopants.[22] All of these manifest themselves in the form of a nonzero magnetization or a hysteresis loop in the plot of the magnetization as a function of the field, making it difficult to isolate the magnetism from the DMS nature. Magnetism from nonmagnetic surface defects is found to be negligible and not considered.[4] The absence of dopant−dopant interactions in the dopant K edge EXAFS spectra (Figure 1b) from similar samples suggests that the observed magnetism cannot arise from the clustering of the dopants. However, it is virtually impossible to assign the magnetization to either the atoms on the surface or the DMS behavior by studying the magnetic properties alone. Additionally, the saturation magnetization (M_S) observed in the literature for different dopants does not follow the trend predicted by the theoretical calculations, making it further challenging to isolate the origin.[4] Hence, the origin of magnetism remains an enigma. The M_S values at 300 K obtained from the literature,[4] plotted as a function of the normalized M−Z_{low} area in Figure 2, clearly point out that the

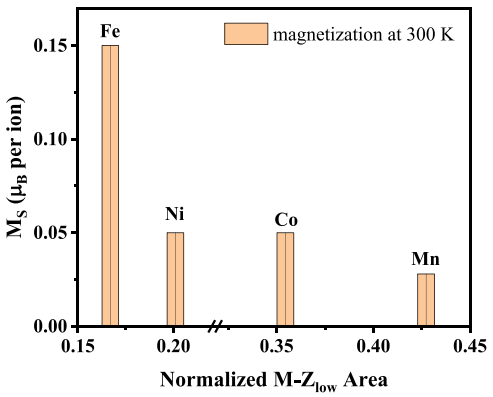

Figure 2. Saturation magnetization of TM-doped CdS as a function of the area under the M−O curve normalized with respect to the total area.

saturation magnetization is inversely proportional to the dopant diffusivity. A decreasing magnetization per dopant ion is consistent with the increasing fraction of dopant ions coordinated to the surface ligands and hence not contributing to the sp−d exchange interaction. Thus, this analysis provides a method to disentangle the contribution of the dopant ions to the magnetism arising from the DMS nature from that of the surface ligand-bound dopant atoms.

While the CN and the M−Z_{low} area provide information on the diffusivity of the ions and magnetism, the M−S bond lengths determine the chemical strain within the system due to the dopant-induced structural perturbations. As shown in Table 1, the iterative fitting model yielded bond length values that match closely with the literature reports of corresponding TM-doped CdS, suggesting that the doping is substitutional. As expected, all the M−S bond lengths are shorter than that of the corresponding Cd−S, as Cd is substituted by a lower atomic numbered element. The central question is whether this guest bond length within the host lattice follows periodic properties. For example, dopant−selenide bond lengths in TM-doped bulk wurtzite CdSe obtained using EXAFS spectroscopy were found to scale with the covalent radii of the dopants, that is, R_{Mn-Se} (2.544 Å) > R_{Fe-Se} (2.498 Å) > R_{Co-Se} (2.439 Å).[36] A more recent density functional theory study on TM-doped 2D CdS nanosheets suggested the necessity to invoke dopants' electronegativity along with the atomic radii to obtain the trend in the bond lengths.[37] However, another computational work on a vast range of TM dopants from 3d, 4d, and 5d series in CdS nanotubes found that the trend is not always systematic.[38] For example, despite sharing the same electronegativity, Ru, Pd, Os, and Ir have different M−S bond lengths ranging between 2.21 and 2.30 Å. Hence, the fundamental physical parameter dictating the variation of the interatomic distance is still an open issue.

As suggested by the earlier reports,[36−38] if the dopant−sulfur bond length was indeed influenced by the covalent radius and the electronegativity, the single parameter containing both

https://doi.org/10.1021/acs.chemmater.2c03776
Chem. Mater. 2023, 35, 2146−2154

information would be the ionic radius. The exact dopant oxidation state in the core of the QDs is important to obtain the necessary ionic radius. Although a linear combination fitting (LCF) in the XANES region of each of the dopants with appropriate standards provides the average oxidation state, since it is not site-specific, it would be impossible to separate the contributions from core and surface coordination. For example, the LCF of the Mn_K edge in Mn-CdS with Mn^{2+} and Mn^{3+} standards yielded an average oxidation state of +2.43 (Figure S5). However, Mn coordinated to both S and Z_{low} contributes to the XANES signal, which makes determining the oxidation state of Mn coordinated to S impossible from LCF. To overcome this problem, we plotted the obtained M−S bond lengths as a function of the dopants' ionic radii in both +2 and +3 states in a tetrahedral configuration as shown in Figure 3. Additionally, in previous studies with identical

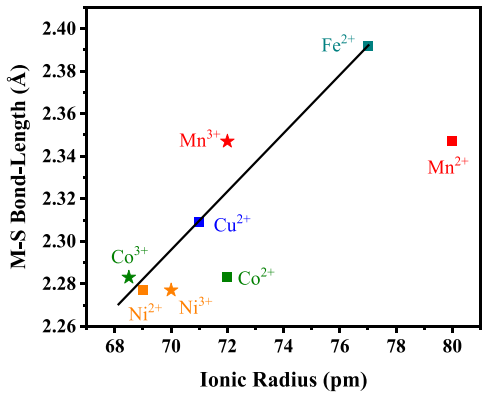

Figure 3. Dopant−sulfur bond length as a function of the ionic radii of dopants, obtained from XAFS data. The solid line connects the bond length values of Fe^{2+} and Cu^{2+} ions.

synthesis conditions,[7,28] it was conclusively proven that Fe and Cu both exist in the +2 oxidation state. We used this information to draw a line joining Fe^{2+} to Cu^{2+}. Following this method, we find that the oxidation state of Ni of +2 is nearly overlapping with that line. Interestingly, Mn and Co's two oxidation states lie on opposite sides of the line, which suggests that both of them have intermediate M−S (M: Mn and Co) bond lengths. The system is therefore in a metastable state with the possibility of switching between two different oxidation states in the case of Mn and Co due to various triggers like photoexcitation.

Signatures of photoinduced switching of the oxidation state of Mn have already been observed in earlier literature.[15] To systematically understand the role of dopants in modulating the exciton dynamics in a series of TM-doped QDs, we studied the carrier relaxation processes using femtosecond TA spectroscopy. We performed a comparative study of the ground state bleach (GSB) growth and recovery dynamics in undoped and doped CdS QDs using a pump fluence of 24 $\mu J/cm^2$ under the nonresonant excitation condition where the photoexcitation energy (3.1 eV) is higher than the bandgap of the QDs and the probe energy is tuned to the bandgap of the sample. Figure 4 represents the differential transmission ($\Delta T/T$) dynamics for undoped and all the doped CdS QDs probed at their respective band edges. The positive $\Delta T/T$ signal is assigned to the GSB of the excitonic transition where we observe a fast rise in the signal followed by an exponential decay holding information about the depopulation and repopulation dynamics of the ground state, respectively.

From the fitting of undoped CdS kinetics, we obtained a finite build-up time of 560 ± 7 fs. This result is in agreement with an earlier study using undoped CdS QDs synthesized via a similar method,[39] where it was observed that the rise of the GSB signal at the band edge is due to the relaxation of the photogenerated charge carriers from the higher vibrational energy levels to the lowest excitonic transition at the band edge, without any intervention from the trap states. The recovery of the charge carriers in undoped CdS can be best fitted with a biexponential decay with a short time constant of 210 ± 65 ps with another very long component (>1 ns) lying outside the timescales of the measurements, suggesting that the QDs are devoid of trap states. This observation is further corroborated by the EXAFS data, which showed that the samples are devoid of trap states.

As expected, the GSB growth dynamics of TM-doped CdS is different from that of the undoped CdS, as shown in Figure 4. While the kinetics of undoped CdS can be satisfactorily fitted with a single exponential build-up and a biexponential recovery, the kinetics of all the TM-doped CdS requires an additional recovery pathway. The GSB growth of TM-doped CdS is faster compared to undoped CdS. It should be noted that only the optically active dopants residing inside the core of the QDs participate in charge or energy transfer processes with the host system. Thus, although the synthesis methods allow dopant diffusion toward the QD surface, the dopants residing on the surface do not take part in the bleach growth or recovery, and accordingly, the rest of the manuscript talks

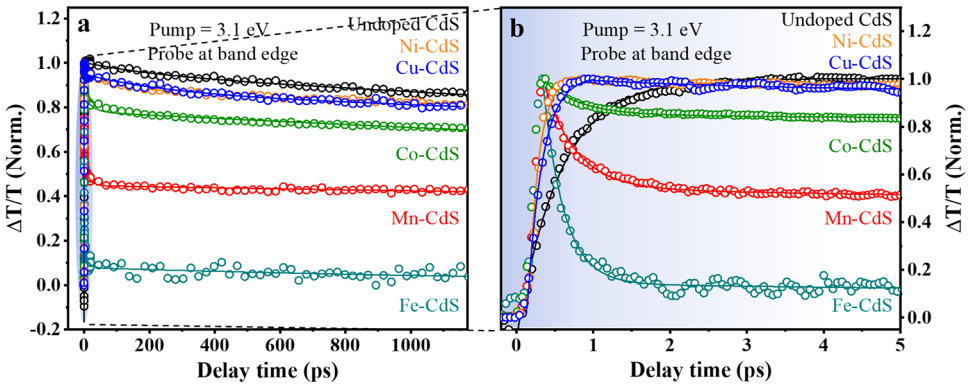

Figure 4. Differential transmission dynamics $\Delta T/T$ as a function of pump−probe delay up to (a) ∼1.2 ns and (b) 5 ps for undoped and TM-doped CdS QDs upon 3.1 eV laser excitation with a pump fluence of 24 $\mu J/cm^2$.

https://doi.org/10.1021/acs.chemmater.2c03776
Chem. Mater. 2023, 35, 2146−2154

Table 2. Fitting Summary of the GSB Recovery Kinetics of Undoped and TM-Doped CdS QDs

sample name	A_1	t_1 (ps)	A_2	t_2 (ps)	A_3	t_3 (ns)
CdS			0.05 ± 0.010	210.00 ± 65.00	0.95 ± 0.010	>1 ns
Mn-CdS	0.50 ± 0.007	0.41 ± 0.009	0.09 ± 0.002	14.40 ± 0.93	0.45 ± 0.002	>1 ns
Fe-CdS	0.85 ± 0.015	0.27 ± 0.008	0.06 ± 0.007	12.75 ± 3.00	0.08 ± 0.006	>1 ns
Co-CdS	0.14 ± 0.003	0.45 ± 0.018	0.07 ± 0.001	24.70 ± 1.26	0.78 ± 0.001	>1 ns
Ni-CdS	0.04 ± 0.001	6.60 ± 0.540	0.07 ± 0.002	118.00 ± 12.20	0.88 ± 0.002	>1 ns
Cu-CdS	0.04 ± 0.002	2.73 ± 0.300	0.08 ± 0.019	257.00 ± 74.00	0.86 ± 0.020	>1 ns

about the optically active dopants.[5,7,9,40,41] GSB growths of Fe-, Mn-, and Co-doped CdS are instantaneous or instrumental response function-limited, whereas CdS samples doped with Ni (125 ± 9 fs) and Cu (200 ± 6 fs) show a relatively slower growth but a bit faster than pristine CdS. The faster growth in doped CdS can be attributed to the presence of alternative depletion channels introduced by doping. It is interesting to note here that the rate of growth at the band edge energy is directly proportional to the number of states introduced by the dopants and hence to the efficiency of the dopants in funneling the charge carriers. For example, while Ni and Cu are known to have one midgap state,[10,42,43] Mn and Co both introduce two midgap states,[9,44,45] and Fe, with its extensive hybridization with the host, has a large number of midgap states with a substantial Fe contribution.[46] The growth rate of the GSB is found to be proportional to the number of midgap states introduced by the dopants.

The results of the fitting of the recovery kinetics are shown in Table 2. The doped CdS NCs follow triexponential recovery where two recovery components involving shorter timescales could be resolved precisely. However, the additional very long-time component, which largely holds information about radiative recombination, does not decay within the time frame of our measurements and hence could not be resolved. It is noteworthy here that the possibility of Auger or trap state recombination is discarded in our analysis because of the absence of surface traps in all the QDs. In the decay kinetics of Cu- and Ni-doped CdS, the fastest recovery component reveals that a fraction of charge carriers is directly captured by the intragap defect states introduced by the dopants. Another recovery component involving a similar timescale with that of undoped CdS suggests that a certain fraction of charge carriers (about 7−8%) is present at the bandgap energy, which in turn is available for recombination through excitonic levels. On the other hand, the timescales involved in the recovery kinetics of Mn- and Co-doped CdS are very much similar to that of Fe-doped CdS. In the case of Fe-CdS, we notice a nearly instantaneous GSB recovery compared to the rest of the timescales involved (Figure 4), similar to our earlier findings.[46] The GSB signal recovers within a few picoseconds (270 ± 8 fs and 12.75 ± 3 ps) as shown in Table 2, which is much faster as compared to undoped CdS having a recovery time constant of 210 ± 65 ps. This drastic difference is due to the presence of multiple acceptor states induced by Fe^{2+} doping.[46] In fact, the initial decay component (270 ± 8 fs) is way faster than the growth time of undoped CdS (560 ± 7 fs), which indicates that the charge carriers are captured by the dopant-induced acceptor states even before they relax down to the host band edges. Due to the high density of states induced by Fe^{2+}, the decay of charge carriers takes place through a continuum of dopant states, which explains the absence of excitonic as well as dopant PL in Fe-doped CdS. Similar to Fe^{2+}, the GSB recovery kinetics of Mn- and Co-doped CdS also displays two lifetimes, substantially faster with respect to the recombination kinetics of undoped CdS. This fast biexponential recovery suggests the ultrafast capture of charge carriers by the dopant states, and the nonavailability of the charge carriers at the bandgap energy explains the absence of excitonic emission in these cases. Thus, the recovery time components and their corresponding intensities determine the availability of charge carriers at the bandgap energy and hence the possibility of excitonic recombination in TM-doped NCs.

As mentioned earlier, Mn and Co are known to provide two midgap states, one near the conduction band and the other near the valence band. Based on our EXAFS analysis, the intermediate M−S bond lengths indicate the feasibility of a transient change in the oxidation state in the case of Mn- and Co-doped CdS. This suggests that the dopant-induced states are more efficient in withdrawing the photoexcited charge carriers from the excitonic states. The exact efficiency of the decay through the dopant levels is dependent on several factors including the band alignment with the host, and it is shown in the previous studies that Mn is efficient in withdrawing the charge carriers from the host.[20,21,45,47,48] Consistent with the above analysis, the GSB recovery kinetics having very fast biexponential recovery suggests the ultrafast capture of charge carriers by the dopant states and hence the possibility of switching between multiple oxidation states, in agreement with our EXAFS analysis. Similar GSB recovery processes occur in Co-CdS except for the fact that the recovery times are slower as compared to Mn-CdS. This is because the energy states introduced by Co are energetically distant (ligand field transition (LFT) energy in Co^{2+}-doped CdS is at ∼728 nm) from the band edges unlike Mn (LFT energy in Mn^{2+}-doped CdS is at ∼585 nm).[40,49−51]

A generalized schematic representation of underlying processes in undoped and TM-doped QDs is depicted in Figure 5.

METHODS

Synthesis and Spectroscopic Characterization. Briefly, after washing the as-synthesized metal sulfide cores, 0.2 M cadmium oleate and 0.2 M sulfur dissolved in 1-octadecene (ODE) were used as precursors to overcoat the CdS matrix over the transition metal sulfide core QDs at a high annealing temperature of 140 °C (250 °C for Fe-CdS). Cd precursors followed by S precursors were injected into the reaction mixture, where each monolayer (ML) shell took 30 min to form. This cycle continued till all the samples achieved sufficient CdS shell thickness (>13 MLs) to ensure that the dopants are diffused throughout the host and the overall dopant amount is less than 5% of Cd. Cu-doped CdS was synthesized by first forming the CdS QDs followed by the addition of 10 μmol of $Cu(St)_2$ solution in 1 mL of ODE at 150 °C and annealing for 2 h. All samples were washed by centrifugation using a mixture of hexane and methanol. The resulting precipitates were redispersed in hexane and used for further spectroscopic studies.

The samples were characterized using XRD, TEM, and optical measurements. Powder XRD patterns for the QDs were recorded on a

https://doi.org/10.1021/acs.chemmater.2c03776
Chem. Mater. 2023, 35, 2146−2154

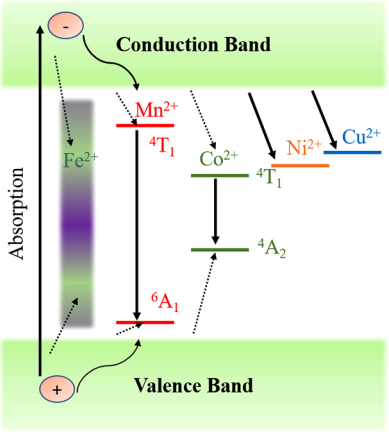

Figure 5. Illustration of various modes of relaxation of charge carriers produced on photoexcitation of the TM-doped QDs.

Bruker D8 Advance diffractometer using Cu Kα radiation (1.5418 Å). TEM was performed on a Tecnai F30 UHR version electron microscope, using a field emission gun (FEG) operating at an accelerating voltage of 200 kV in the bright-field mode using Cu-coated holey carbon TEM grids. Absorption spectra of samples were recorded using an Agilent 8453 UV−visible spectrometer. Steady-state photoluminescence spectra were collected using a 450 W xenon lamp as the source on an FLSP920 spectrometer, Edinburgh Instruments.

Extended X-ray Absorption Fine Structure (EXAFS) Spectroscopy. EXAFS spectroscopic measurements were carried out at the P64 beamline at PETRA III, DESY in Hamburg, Germany. All the measurements were made in reflection geometry in the fluorescence mode on thin films. X-ray energy was calibrated to 26,711, 6539, 7112, 7709, 8333, and 8979 eV for Cd_K, Mn_K, Fe_K, Co_K, Ni_K, and Cu_K measurements, respectively.

Data were processed using Athena[29] software plotting the EXAFS oscillation $\chi(k)$ in wavenumber (k) space as a function of the photoelectron wavenumber k and then Fourier transforming in position (R) space through a Hanning window for the visual representation of the bond lengths involved in the system. After the edge energies were calibrated to the respective metal foil energies, several scans for each data were merged to get better-quality data before fitting them to theoretical standards, which were analyzed with the fitting software Artemis[29] to get quantitative information about the local environment of the NCs. Throughout the analysis, the theoretical standards to which the experimental data were fitted were generated from FEFF6 built into Artemis within a cluster size of 7 Å.

The theoretical standards for dopant_K edge analysis were generated from an FEFF input file obtained by replacing Cd atoms with dopant atoms changing the lattice parameters of hexagonal CdS calculated from the bond lengths of respective dopant−sulfur and using simple geometric arguments to obtain the revised lattice parameters. The modeling-obtained bond lengths were then taken, and the lattice parameters were recalculated. This process was repeated till good matches of the dopant−sulfur bond lengths with literature reports were obtained and the overall statistical qualities of the fit (R-factors) became reliable. The final step of the iteration is used for all the calculations.

Transient Absorption Measurement. Ultrafast transient absorption measurements were performed exploiting an amplified Ti:sapphire laser (Coherent Libra) generating 100 fs pulses at 800 nm and a 2 kHz repetition rate. Pump pulses at 400 nm were generated by frequency doubling the fundamental wavelength by a 2 mm-thick β-barium borate crystal; they were modulated at 1 kHz by a mechanical chopper and focused in a 270 μm diameter spot on the samples dispersed in hexane. Pump pulse power was adjusted to perform the experiments at a fluence of 24 $\mu J/cm^2$. UV−visible probe pulses were produced via white-light supercontinuum generation by focusing part of the fundamental beam in a calcium fluoride plate. Chirp-free differential transmission spectra $\Delta T/T = (T_{on} - T_{off})/T_{off}$, T_{on} and T_{off} being the transmission of the probe through the perturbed and unperturbed samples, were acquired at different pump−probe delays by a fast optical multichannel analyzer operating at the full laser repetition rate. The temporal resolution of the setup was ∼100 fs. All the measurements were carried out at room temperature.

CONCLUSIONS

In summary, we have studied the dopant-induced structural perturbation and carrier dynamics in various TM-doped CdS QDs via the combination of EXAFS and ultrafast TA spectroscopies. We find that dilute doping does not create structural perturbations in the Cd sites and does not cause dopant clustering. The nature of the diffusion across the dopants is predicted, which in turn explains that the dopant-induced magnetism in CdS QDs is DMS in nature arising out of host−dopant interactions and not from the surface traps or dopant clustering. We show that the oxidation states play a central role in the arrangement of the dopant−sulfur bond lengths in a periodic trend as a function of dopants' ionic radii. This procedure is lattice site-selective unlike XANES, which can be used to get a qualitative estimate of the oxidation states, which in turn predicts that some dopants (Mn and Co) can switch between multiple oxidation states, an observation further verified by femtosecond transient absorption spectroscopy.

ASSOCIATED CONTENT

Supporting Information

The Supporting Information is available free of charge at https://pubs.acs.org/doi/10.1021/acs.chemmater.2c03776.

XRD patterns, UV−visible spectra, PL spectra, and Cd_K edge XANES and EXAFS of doped CdS; HRTEM image and linear combination fitting (LCF) of XANES of Mn-doped CdS; list of XAFS fitting parameters for Cd_K and dopant K edges for all samples (PDF)

AUTHOR INFORMATION

Corresponding Author

Ranjani Viswanatha − *New Chemistry Unit and International Centre for Materials Science, Jawaharlal Nehru Centre for Advanced Scientific Research, Bangalore 560064, India;* orcid.org/0000-0002-3819-4029; Email: rv@jncasr.ac.in

Authors

Saptarshi Chakraborty − *New Chemistry Unit, Jawaharlal Nehru Centre for Advanced Scientific Research, Bangalore 560064, India;* orcid.org/0000-0001-8559-1089

Payel Mondal − *New Chemistry Unit, Jawaharlal Nehru Centre for Advanced Scientific Research, Bangalore 560064, India;* orcid.org/0000-0002-2703-1734

Mahima Makkar − *New Chemistry Unit, Jawaharlal Nehru Centre for Advanced Scientific Research, Bangalore 560064, India;* orcid.org/0000-0002-2804-9733

Luca Moretti − *IFN-CNR, Dipartimento di Fisica, Politecnico di Milano, 20133 Milano, Italy;* orcid.org/0000-0001-8092-0752

Giulio Cerullo − *IFN-CNR, Dipartimento di Fisica, Politecnico di Milano, 20133 Milano, Italy;* orcid.org/0000-0002-9534-2702

Complete contact information is available at:
https://pubs.acs.org/10.1021/acs.chemmater.2c03776

Author Contributions

‖S.C. and P.M. contributed equally to this work.

Notes

The authors declare no competing financial interest.

■ ACKNOWLEDGMENTS

We thank JNCASR for providing experimental facilities. S.C., P.M., and M.M. acknowledge DST-INSPIRE, CSIR, and JNCASR for research fellowships, respectively. R.V. is grateful for the partial support from the SERB POWER fellowship. EXAFS measurements were carried out in the P64 beamline at PETRA III of DESY, a member of the Helmholtz Association (HGF), Germany. The authors thank Dr. Wolfgang A. Caliebe and Dr. V. Murzin for beamline assistance. Financial support by the Department of Science and Technology (Government of India) provided within the framework of India@DESY collaboration is gratefully acknowledged.

■ REFERENCES

(1) Fainblat, R.; Barrows, C. J.; Gamelin, D. R. Single Magnetic Impurities in Colloidal Quantum Dots and Magic-Size Clusters. *Chem. Mater.* **2017**, *29*, 8023−8036.
(2) Pradhan, N.; Das Adhikari, S.; Nag, A.; Sarma, D. D. Luminescence, Plasmonic, and Magnetic Properties of Doped Semiconductor Nanocrystals. *Angew. Chem., Int. Ed.* **2017**, *56*, 7038−7054.
(3) Umebayashi, T.; Yamaki, T.; Itoh, H.; Asai, K. Analysis of electronic structures of 3d transition metal-doped TiO_2 based on band calculations. *J. Phys. Chem. Solids* **2002**, *63*, 1909−1920.
(4) Saha, A.; Makkar, M.; Shetty, A.; Gahlot, K.; Pavan, A. R.; Viswanatha, R. Diffusion doping in quantum dots: bond strength and diffusivity. *Nanoscale* **2017**, *9*, 2806−2813.
(5) Grandhi, G. K.; Tomar, R.; Viswanatha, R. Study of Surface and Bulk Electronic Structure of II−VI Semiconductor Nanocrystals Using Cu as a Nanosensor. *ACS Nano* **2012**, *6*, 9751−9763.
(6) Pradhan, N.; Goorskey, D.; Thessing, J.; Peng, X. An Alternative of CdSe Nanocrystal Emitters: Pure and Tunable Impurity Emissions in ZnSe Nanocrystals. *J. Am. Chem. Soc.* **2005**, *127*, 17586−17587.
(7) Mondal, P.; Chakraborty, S.; Grandhi, G. K.; Viswanatha, R. Copper Doping in II−VI Semiconductor Nanocrystals: Single-Particle Fluorescence Study. *J. Phys. Chem. Lett.* **2020**, *11*, 5367−5372.
(8) Su, F. H.; Fang, Z. L.; Ma, B. S.; Ding, K.; Li, G. H.; Xu, S. J. Temperature and pressure behavior of the emission bands from Mn-, Cu-, and Eu-doped ZnS nanocrystals. *J. Appl. Phys.* **2004**, *95*, 3344−3349.
(9) Norris, D. J.; Yao, N.; Charnock, F. T.; Kennedy, T. A. High-quality manganese-doped ZnSe nanocrystals. *Nano Lett.* **2001**, *1*, 3−7.
(10) Jana, S.; Srivastava, B. B.; Jana, S.; Bose, R.; Pradhan, N. Multifunctional doped semiconductor nanocrystals. *J. Phys. Chem. Lett.* **2012**, *3*, 2535−2540.
(11) Nag, A.; Cherian, R.; Mahadevan, P.; Gopal, A. V.; Hazarika, A.; Mohan, A.; Vengurlekar, A. S.; Sarma, D. D. Size-dependent tuning of Mn2+ d emission in Mn2+−doped CdS nanocrystals: bulk vs surface. *J. Phys. Chem. C* **2010**, *114*, 18323−18329.
(12) Bhargava, R. N.; Gallagher, D.; Hong, X.; Nurmikko, A. Optical Properties of Manganese-Doped Nanocrystals of ZnS. *Phys. Rev. Lett.* **1994**, *72*, 416.
(13) Beaulac, R.; Archer, P. I.; Ochsenbein, S. T.; Gamelin, D. R. Mn^{2+}-Doped CdSe Quantum Dots: New Inorganic Materials for Spin-Electronics and Spin-Photonics. *Adv. Funct. Mater.* **2008**, *18*, 3873−3891.
(14) Bol, A. A.; Meijerink, A. Long-Lived Mn^{2+} Emission in Nanocrystalline ZnS: Mn^{2+}. *Phys. Rev. B* **1998**, *58*, No. R15997.
(15) Gahlot, K.; P, K. R.; Camellini, A.; Sirigu, G.; Cerullo, G.; Zavelani-Rossi, M.; Singh, A.; Waghmare, U. V.; Viswanatha, R. Transient Species Mediating Energy Transfer to Spin-Forbidden Mn d States in II−VI Semiconductor Quantum Dots. *ACS Energy Lett.* **2019**, *4*, 729−735.
(16) Cherepanov, D.; Kostrov, A.; Gostev, F.; Shelaev, I.; Motyakin, M.; Kochev, S.; Kabachii, Y.; Nadtochenko, V. Ultrafast Quenching of Excitons in the $Zn_xCd_{1-x}S$/ZnS Quantum Dots Doped with Mn^{2+} through Charge Transfer Intermediates Results in Manganese Luminescence. *Nanomaterials* **2021**, *11*, 3007.
(17) P, K. R.; Viswanatha, R. Mechanism of Mn emission: Energy transfer vs charge transfer dynamics in Mn-doped quantum dots. *APL Mater.* **2020**, *8*, No. 020901.
(18) Chen, H.-Y.; Son, D. H. Energy and Charge Transfer Dynamics in Doped Semiconductor Nanocrystals. *Isr. J. Chem.* **2012**, *52*, 1016−1026.
(19) Hsia, C.-H.; Wuttig, A.; Yang, H. An Accessible Approach to Preparing Water-Soluble Mn^{2+}-Doped (CdSSe) ZnS (Core) Shell Nanocrystals for Ratiometric Temperature Sensing. *ACS Nano* **2011**, *5*, 9511−9522.
(20) Chen, H.-Y.; Chen, T.-Y.; Son, D. H. Measurement of Energy Transfer Time in Colloidal Mn-Doped Semiconductor Nanocrystals. *J. Phys. Chem. C* **2010**, *114*, 4418−4423.
(21) Chen, H.-Y.; Maiti, S.; Son, D. H. Doping Location-Dependent Energy Transfer Dynamics in Mn-Doped CdS/ZnS Nanocrystals. *ACS Nano* **2012**, *6*, 583−591.
(22) Makkar, M.; Viswanatha, R. Recent Advances in Magnetic Ion-Doped Semiconductor Quantum Dots. *Curr. Sci.* **2017**, *112*, 1421−1429.
(23) Pan, F.; Song, C.; Liu, X. J.; Yang, Y. C.; Zeng, F. Ferromagnetism and possible application in spintronics of transition-metal-doped ZnO films. *Mater. Sci. Eng. R Rep.* **2008**, *62*, 1−35.
(24) Wang, L.; Chen, Z.; Liang, G.; Li, Y.; Lai, R.; Ding, T.; Wu, K. Observation of a Phonon Bottleneck in Copper-Doped Colloidal Quantum Dots. *Nat. Commun.* **2019**, *10*, 1−8.
(25) Gao, Y.; Liu, H.; Li, J.; Xiao, S.; Guo, Z.; Pan, R.; Lin, X.; He, T. Efficient Multiphoton Absorption of Near-Infrared Emitting Cu-Doped ZnInS/ZnS Nanocrystals. *J. Phys. D: Appl. Phys.* **2020**, *53*, 255103.
(26) Ye, Y.; Wang, X.; Ye, S.; Xu, Y.; Feng, Z.; Li, C. Charge-Transfer Dynamics Promoted by Hole Trap States in CdSe Quantum Dots−Ni^{2+} Photocatalytic System. *J. Phys. Chem. C* **2017**, *121*, 17112−17120.
(27) Maiti, S.; Dana, J.; Jadhav, Y.; Debnath, T.; Haram, S. K.; Ghosh, H. N. Electrochemical Evaluation of Dopant Energetics and the Modulation of Ultrafast Carrier Dynamics in Cu-doped CdSe Nanocrystals. *J. Phys. Chem. C* **2017**, *121*, 27233−27240.
(28) Saha, A.; Shetty, A.; Pavan, A. R.; Chattopadhyay, S.; Shibata, T.; Viswanatha, R. Uniform Doping in Quantum-Dots-Based Dilute Magnetic Semiconductor. *J. Phys. Chem. Lett.* **2016**, *7*, 2420−2428.
(29) Ravel, B.; Newville, M. ATHENA, ARTEMIS, HEPHAESTUS: data analysis for X-ray absorption spectroscopy using IFEFFIT. *J. Synchrotron Rad.* **2005**, *12*, 537−541.
(30) Saha, A.; Chattopadhyay, S.; Shibata, T.; Viswanatha, R. Core−Shell to Doped Quantum Dots: Evolution of the Local Environment Using XAFS. *J. Phys. Chem. C* **2016**, *120*, 18945−18951.
(31) Bürger, D.; Seeger, M.; Zhou, S.; Skorupa, W.; Schmidt, H. Transition metal diffusion in diluted magnetic Si and GaAs prepared by pulsed laser processing. *J. Appl. Phys.* **2012**, *111*, No. 054914.
(32) Nabi, A.; Akhtar, Z.; Iqbal, T.; Ali, A.; Arshad Javid, M. The electronic and magnetic properties of wurtzite Mn:CdS, Cr:CdS Mn:Cr:CdS: first principles calculations. *J. Semicond.* **2017**, *38*, No. 073001.
(33) Maity, P.; Kumar, S.; Kumar, R.; Jha, S. N.; Bhattacharyya, D.; Barman, S. R.; Chatterjee, S.; Pal, B. N.; Ghosh, A. K. Role of Cobalt Doping in CdS Quantum Dots for Potential Application in Thin Film Optoelectronic Devices. *J. Phys. Chem. C* **2021**, *125*, 2074−2088.

(34) Li, P.; Zhang, C.-w.; Lian, J.; Ren, M.-j.; Wang, P.-j.; Yu, X.-h.; Gao, S. First-principle study of optical properties of Cu-doped CdS. *Opt. Commun.* **2013**, *295*, 45−52.
(35) Madhu, C.; Sundaresan, A.; Rao, C. N. R. Room-temperature ferromagnetism in undoped **GaN** and **CdS** semiconductor nanoparticles. *Phys. Rev. B* **2008**, *77*, No. 201306.
(36) Lawniczak-Jablonska, K.; Libera, J.; Iwanowski, R. J. EXAFS determination of local atomic structure of selected transition metals in CdSe matrix. *J. Alloys Compd.* **1999**, *286*, 89−92.
(37) Chen, X.; Li, P.; Ren, M.; Wang, P. First-Principles Study on the Electronic, Magnetic, and Optical Properties in TM Atom Doped Cadmium Sulfide Nanosheets. *Phys. Status Solidi B* **2019**, *256*, No. 1900182.
(38) Garg, P.; Nair, A. S.; Rawat, K. S.; Pathak, B. Computational Screening of Electrocatalytic Activity of Transition Metal-Doped CdS Nanotubes for Water Splitting. *J. Phys. Chem. C* **2019**, *123*, 13419−13427.
(39) Makkar, M.; Moretti, L.; Maiuri, M.; Cerullo, G.; Viswanatha, R. Ultrafast Electron−Hole Relaxation Dynamics in CdS Nanocrystals. *J. Phys.: Mater.* **2021**, *4*, No. 034005.
(40) Zeng, R.; Rutherford, M.; Xie, R.; Zou, B.; Peng, X. Synthesis of Highly Emissive Mn-Doped ZnSe Nanocrystals Without Pyrophoric Reagents. *Chem. Mater.* **2010**, *22*, 2107−2113.
(41) Pradhan, N.; Peng, X. Efficient and Color-Tunable Mn-Doped ZnSe Nanocrystal Emitters: Control of Optical Performance via Greener Synthetic Chemistry. *J. Am. Chem. Soc.* **2007**, *129*, 3339−3347.
(42) Nelson, H. D.; Hinterding, S. O. M.; Fainblat, R.; Creutz, S. E.; Li, X.; Gamelin, D. R. Mid-gap States and Normal vs Inverted Bonding in Luminescent Cu^{+}-and Ag^{+}-doped CdSe Nanocrystals. *J. Am. Chem. Soc.* **2017**, *139*, 6411−6421.
(43) Srivastava, B. B.; Jana, S.; Pradhan, N. Doping Cu in Semiconductor Nanocrystals: Some Old and Some New Physical Insights. *J. Am. Chem. Soc.* **2011**, *133*, 1007−1015.
(44) May, J. W.; Ma, J.; Badaeva, E.; Li, X. Effect of Excited-State Structural Relaxation on Midgap Excitations in Co^{2+}-Doped ZnO Quantum Dots. *J. Phys. Chem. C* **2014**, *118*, 13152−13156.
(45) Santra, P. K.; Kamat, P. V. Mn-Doped Quantum Dot Sensitized Solar Cells: A Strategy to Boost Efficiency over 5%. *J. Am. Chem. Soc.* **2012**, *134*, 2508−2511.
(46) Makkar, M.; Dheer, L.; Singh, A.; Moretti, L.; Maiuri, M.; Ghosh, S.; Cerullo, G.; Waghmare, U. V.; Viswanatha, R. Magneto-Optical Stark Effect in Fe-Doped CdS Nanocrystals. *Nano Lett.* **2021**, *21*, 3798−3804.
(47) Debnath, T.; Maity, P.; Maiti, S.; Ghosh, H. N. Electron Trap to Electron Storage Center in Specially Aligned Mn-Doped CdSe d-Dot: A Step Forward in the Design of Higher Efficient Quantum-Dot Solar Cell. *J. Phys. Chem. Lett.* **2014**, *5*, 2836−2842.
(48) Pradhan, N.; Sarma, D. D. Advances in Light-Emitting Doped Semiconductor Nanocrystals. *J. Phys. Chem. Lett.* **2011**, *2*, 2818−2826.
(49) Yang, Y.; Chen, O.; Angerhofer, A.; Cao, Y. C. Radial-Position-Controlled Doping in CdS/ZnS Core/Shell Nanocrystals. *J. Am. Chem. Soc.* **2006**, *128*, 12428−12429.
(50) Zhang, W.; Li, Y.; Zhang, H.; Zhou, X.; Zhong, X. Facile Synthesis of Highly Luminescent Mn-Doped ZnS Nanocrystals. *Inorg. Chem.* **2011**, *50*, 10432−10438.
(51) Norberg, N. S.; Dalpian, G. M.; Chelikowsky, J. R.; Gamelin, D. R. Energetic Pinning of Magnetic Impurity Levels in Quantum-Confined Semiconductors. *Nano Lett.* **2006**, *6*, 2887−2892.

https://doi.org/10.1021/acs.chemmater.2c03776
Chem. Mater. 2023, 35, 2146−2154